LIMNOLOGY and OCEANOGRAPHY

ASLO

Limnol. Oceanogr. 67, 2022, 419–433

doi: 10.1002/lno.12001

Enhanced benthic nitrous oxide and ammonium production after natural oxygenation of long-term anoxic sediments

Astrid Hylén,[1*] **Stefano Bonaglia**,[1,2,3] **Elizabeth Robertson**,[1] **Ugo Marzocchi**,[4,5] **Mikhail Kononets**,[1] **Per O. J. Hall**[1]

[1]Department of Marine Sciences, University of Gothenburg, Gothenburg, Sweden
[2]Department of Ecology, Environment and Plant Sciences, Stockholm University, Stockholm, Sweden
[3]Nordcee, Department of Biology, University of Southern Denmark, Odense, Denmark
[4]Center for Electromicrobiology, Department of Biosciences, Aarhus University, Aarhus, Denmark
[5]Center for Water Technology (WATEC), Department of Biosciences, Aarhus University, Aarhus, Denmark

Abstract

Coastal and shelf sediments are central in the global nitrogen (N) cycle as important sites for the removal of fixed N. However, this ecosystem service can be hampered by ongoing deoxygenation in many coastal areas. Natural reoxygenation could reinstate anoxic sediments as sites where fixed N is removed efficiently. To investigate this further, we studied benthic N cycling in previously long-term anoxic sediments, following a large intrusion of oxygenated water to the Baltic Sea. During three campaigns in 2016–2018, we measured in situ sediment–water fluxes of ammonium (NH_4^+), nitrate (NO_3^-), oxygen (O_2), dissolved inorganic carbon, and NO_3^- reduction processes using benthic chamber landers. Sediment microprofiles of O_2, nitrous oxide (N_2O), and hydrogen sulfide were measured in sediment cores. At a permanently oxic station, denitrification to N_2 was the main NO_3^- reduction process. Benthic N_2O production appeared to be linked to nitrification, although no net N_2O fluxes from the sediment were detected. At newly oxygenated sites, dissimilatory NO_3^- reduction to NH_4^+ comprised almost half of the total NO_3^- reduction. At these stations, the removal of fixed N was inefficient due to high effluxes of NH_4^+. Sedimentary N_2O production was associated with incomplete denitrification, accounting for 41–88% of the total denitrification rate. Microprofiling revealed algae aggregates as potential hotspots of seafloor N_2O production. Our results show that transient oxygenation of euxinic systems initiates benthic NO_3^- reduction, but may not lead to efficient sedimentary removal of fixed N. Instead, recycling of N compounds is promoted, which may accelerate the return to anoxia.

The doubling of fixed nitrogen (N) inputs to the ocean via rivers and the atmosphere since pre-industrial times (Seitzinger et al. 2010; Beusen et al. 2016; Jickells et al. 2017) has resulted in a strong research focus on the processes affecting the fate of fixed N in the marine environment (Seitzinger et al. 2006; Galloway et al. 2008; Voss et al. 2013). In this respect, coastal sediments play an important role as they receive large amounts of N from land and are sites of intense N cycling. It is estimated that at least 25% of the global marine fixed N loss takes place in coastal and shelf sediments (Voss et al. 2013), even though they comprise only ~ 8% of the global seafloor area (Sarmiento and Gruber 2006). However, coastal zones globally are under pressure from the spread of oxygen (O_2) depletion (Diaz and Rosenberg 2008; Altieri and Gedan 2015; Breitburg et al. 2018). Oxygen exerts a strong control on the N cycle by activating or suppressing many of the microbial processes involved in N transformation (Canfield et al. 2005; Thamdrup and Dalsgaard 2008; Kuypers et al. 2018). A key question is thus how changing O_2 conditions in coastal areas will affect the rates of and partitioning between processes in the N cycle, and ultimately the fate of fixed N in the ocean.

Under oxic conditions, ammonium (NH_4^+) produced during degradation of organic matter is oxidized to nitrite (NO_2^-) and nitrate (NO_3^-) by nitrifying bacteria. Any NO_2^- and NO_3^- (here collectively called NO_x^-) entering an anoxic environment can

*Correspondence: astrid.hylen@marine.gu.se

Additional Supporting Information may be found in the online version of this article.

Author Contribution Statement: AH, SB, and PH designed the study. AH, SB, and ER conducted sediment sampling, ^{15}N incubations and sample analysis. SB and UM conducted microprofile measurements. MK coordinated the lander deployments. AH, SB, and ER interpreted the data and wrote the manuscript with input from all authors.

be used as an electron acceptor in one of three NO_x^- reduction processes: denitrification, anaerobic ammonium oxidation (anammox), and dissimilatory nitrate reduction to ammonium (DNRA). Of these respiratory processes, denitrification and anammox constitute sinks for fixed N by reducing NO_x^- to gaseous N_2, while during DNRA, NO_x^- is instead converted back to readily bioavailable NH_4^+, thereby keeping fixed N in the system (Canfield et al. 2005; Giblin et al. 2013).

Although these NO_x^- reduction processes take place in anoxic environments, they are indirectly dependent on O_2 for the supply of NO_x^-. In long-term anoxic systems where NO_x^- is depleted, oxygenation events can promote removal of fixed N by activating nitrification which supplies NO_x^- for denitrification and anammox (De Brabandere et al. 2015). Denitrification is commonly the major N removal process in coastal sediments due to high availability of organic matter in coastal systems, favoring heterotrophic denitrification over autotrophic anammox as N_2 production process (Devol 2015). However, DNRA appears to be important in highly reduced sediment, especially where the NO_x^- concentration is low relative to the electron donor (Kraft et al. 2014; Hardison et al. 2015; Kessler et al. 2018). Furthermore, hydrogen sulfide (H_2S), which is often prevalent in sediments of previously long-term anoxic coastal systems, may inhibit denitrification and anammox, thus slowing down these processes or leading to accumulation of intermediates such as the strong greenhouse gas nitrous oxide (N_2O) in the case of denitrification (Sørensen et al. 1980; Senga et al. 2006; Jensen et al. 2008). Some organisms that carry out DNRA can couple the process to H_2S oxidation (Fossing et al. 1995) or instead reduce sulfate (Dalsgaard and Bak 1994), however, and so are more tolerant to (or even dependent upon) H_2S.

Recently, benthic NO_x^- reduction processes were studied during forced oxygenation of the long-term anoxic By Fjord in Sweden (De Brabandere et al. 2015). DNRA was initially the dominant NO_x^- reduction process, but denitrification became increasingly important with time and eventually became the main NO_x^- reduction process. Although insightful, the study does not necessarily describe natural conditions since the system was kept artificially oxygenated continually for 2 yr, substantially longer than natural oxygenation events last in similar systems (by Fjord, De Brabandere et al. 2015; Baltic Sea, Meier et al. 2018; Saanich Inlet, Michiels et al. 2019). However, a natural oxygenation event in the long-term anoxic Baltic Sea recently offered a unique chance to study the onset of NO_x^- reduction processes. After 10 yr of O_2 depletion, a so-called Major Baltic Inflow (MBI) brought oxygenated water to the long-term anoxic bottom waters of the central Baltic Sea. Three months after the MBI reached the Eastern Gotland Basin in the central Baltic Sea, Hall et al. (2017) observed an increase in the bottom water NO_x^- concentration from <0.5 to ~ 10 μM. During these initial samplings, measurements of NO_x^- reduction process rates showed a dominance of DNRA over denitrification.

In this study, we describe the long-term impact of this natural oxygenation event on the fate of fixed N in the sediment. Our goals were to investigate (1) whether the newly oxygenated sediments were sites of efficient removal of fixed N through denitrification and anammox, (2) which environmental factors affected the division between NO_x^- reduction processes, and (3) whether NO_x^- from the water column or sedimentary nitrification was fuelling NO_x^- reduction processes in the sediment. To this end, we conducted three yearly samplings in 2016, 2017, and 2018 where we performed in situ measurements of NO_x^- reduction process rates and sediment–water fluxes of nutrients, O_2, and dissolved inorganic carbon (DIC). We additionally collected sediment samples and measured sediment microprofiles of O_2, N_2O, and H_2S to gain further insights into the spatial distribution of the processes in surface sediments.

Material and methods

Study site

The Baltic Sea is a semi-enclosed brackish water sea in Northern Europe (Fig. 1a). The central and southern parts of the Baltic Sea are naturally prone to hypoxia due to slow water exchange and strong water column stratification (Liblik et al. 2018). The situation has been worsened by decades of anthropogenic nutrient release from land, causing eutrophication which in turn has led to extensive O_2 depletion (Carstensen et al. 2014). Every few years, the deep water in the Baltic Sea is ventilated by large inflows, MBIs. After a stagnation period of 10 yr, the third largest MBI in 60 yr took place in December 2014 and brought O_2 to long-term anoxic parts of the Baltic Sea (Liblik et al. 2018).

The MBI reached the Eastern Gotland Basin in the central Baltic Sea in March 2015 (Fig. 1b; Liblik et al. 2018). The water column in the Eastern Gotland Basin is normally O_2 depleted below the halocline at 60–80 m depth, but the inflow created a layer of oxygenated water between 140 m depth and the seafloor (maximum depth 249 m; Hall et al. 2017). This O_2 was consumed within 6 months, but another inflow in January 2016 oxygenated the area again until May (Liblik et al. 2018). In 2014–2017, several small inflows also brought O_2 to the layer between the halocline and 170 m depth (Fig. 1b; SMHI 2021).

We conducted yearly samplings at four stations in the Eastern Gotland Basin in April 2016–2018, along a depth transect from the island of Gotland toward the deepest part of the basin (Fig. 1a). Sta. A is situated at 60 m depth and is permanently oxic. Stas. D, E, and F were oxygenated at different times during the sampling campaign (Fig. 1b, Table 1). Stas. E (170 m) and F (210 m) were oxygenated by the MBI and following inflows. These stations became anoxic again in 2018 and 2017, respectively. Sta. D (130 m) was anoxic during our sampling in 2016, but had likely been oxygenated briefly prior to our visit (Sommer et al. 2017; SMHI 2021). The site was reached by an oxic inflow in 2017, but was anoxic again in 2018.

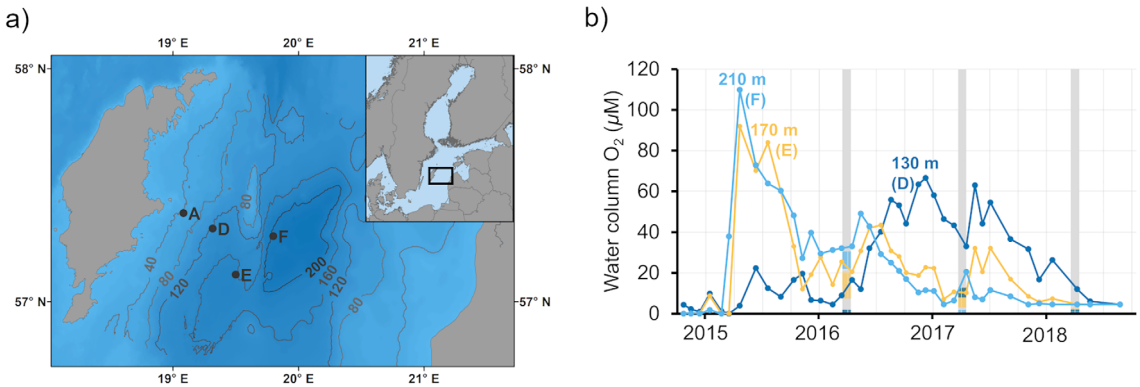

Fig. 1. Description of the study sites. (**a**) Map of the study sites in the Eastern Gotland Basin, the Baltic Sea. Contour lines show depths. (**b**) Water column O_2 concentrations at the depths of the newly oxygenated stations. Measurements by the Swedish Meteorological and Hydrological Institute (SMHI 2021) at the monitoring Sta. BY15, which is situated close to Sta. F. Gray bars mark sampling occasions in this study, bottom water O_2 concentrations measured by the benthic chamber landers are shown on the bars. The O_2 concentration at Sta. A (60 m depth) was 100–345 μM (70 μM at one occasion) during the period (SMHI 2021).

Sediment properties and microsensor measurements

Sediment cores for analysis of solid-phase carbon (C) and N were collected with a multiple corer (inner Ø 9.9 cm). The cores were vertically sectioned in 0.5, 1, or 2 cm intervals down to a sediment depth of 20 cm, with highest resolution at the top. The samples were freeze dried and homogenized using mortar and pestle prior to analysis. Due to technical issues, there are no solid phase samples from 2018. Sediment cores for pore-water sampling were processed under anoxic conditions in an N_2-filled glove bag. Sediment cores were sectioned in the same intervals as described above, before extraction of pore water using Rhizon samplers (Rhizon SMS, Rhizosphere). Samples were stored dark and cold until analysis.

Sediment depth microprofiles of O_2, H_2S, and N_2O (only 2017 and 2018) were measured in cores (inner Ø 5 cm) collected from a modified box corer (Blomqvist et al. 2015) and transferred to a 10 L aquarium where they were kept at in situ temperature and O_2 concentration. Within a few hours of sediment retrieval, microprofiles were measured as described by Marzocchi et al. (2018a), using microsensors (Revsbech 1989; Kühl et al. 1998; Andersen et al. 2001) constructed at Aarhus University. At each station, 3–5 microprofiles were measured in each replicate core (n = 2–3 for Stas. A, D, and F, and n = 1 for Sta. E). Due to sensor breakage, no N_2O profiles were measured at Stas. F and A in 2017 or Sta. D in 2018. In 2017, O_2 and N_2O were also measured in three aggregates of algal material deposited on the sediment surface of cores from Sta. E.

Lander incubations

Benthic solute fluxes were measured in situ using the Gothenburg benthic chamber landers. Deployment of the landers

Table 1. Station information, bottom water properties and solid phase data. NO_x^- red. measurement: C = cores, S = slurry, L = benthic chamber lander. Core and slurry incubations were only used to correct rates measured with the benthic chamber lander. Values of sedimentary OC and N are averages for the top 2 cm; there are no samples from 2018.

Stations	Year	NO_x^- red. meas.	Salinity	Temp (°C)	O_2 (μM)	NO_x^- (μM)	OC (%)	N (%)	OC : N (mol:mol)
A	2016		7.3–7.4	3.6–3.9	330–350	2.9–3.3	0.9	0.1	10.5
	2017	C, L, S	7.7–8.9	4.0–5.0	100–300	3.3–8.6	1.2	0.2	7.0
	2018	L	7.4–7.5	2.6–3.0	325–355	2.9–3.3			
D	2016	C, L	12.5–12.7	6.5–6.6	< 0.5	0.2–0.8	7.9	0.9	10.2
	2017	L, S	12.7	6.7–6.8	8–13	7.3–8.0	10.5	1.3	9.4
	2018	L	12.4–12.6	6.6–6.9	< 0.5	2.6–2.7			
E	2016	C, L	12.9–13.1	6.8–6.9	7–20	8.3–11.9	12.1	1.3	10.9
	2017	L	13.1	6.9–7.2	3–13	2.0–6.3	10.1	1.2	9.8
	2018		13.1	6.8–7.1	< 0.5	0.03–0.19			
F	2016	C, L	13.8–13.9	7.3–7.4	22–30	9.7–11.0	12.1	1.3	10.9
	2017		13.5	7.2–7.4	< 0.5	0.03–0.07	11.7	1.4	9.7
	2018		13.1–13.3	6.9–7.15	< 0.5	0.09–0.18			

has been described in detail elsewhere (Kononets et al. 2021). Briefly, the big and small landers were equipped with four and two incubation chamber modules, respectively. Sediment and bottom waters were incubated for 36 h at Sta. A and 14 h at Stas. D–F. The conditions inside and outside the chambers were monitored with O_2 optodes (Model 3830; Aanderaa Data Instruments) and conductivity and temperature sensors (Model 3919; Aanderaa Data Instruments). Chambers that initially contained O_2 did not become anoxic during the incubations. Nine water samples per chamber were collected with syringes at preset times; water from the syringes was processed immediately after lander recovery. Nutrient samples were filtered through pre-cleaned syringe filters (cellulose acetate, 0.45 μm pore size), and were thereafter kept refrigerated until analysis immediately after the cruises. Samples for DIC were analyzed onboard.

In half of the chambers, denitrification and DNRA were measured following the protocol of De Brabandere et al. (2015) with minor modifications. A sample was withdrawn 10 min after the start of the incubation. After 10 more minutes, a solution of $Na^{15}NO_3^-$ (99.4 atom%, Sigma-Aldrich) in Milli-Q water was injected into the chambers, increasing the in situ concentration of NO_3^- by $\sim 70\,\mu$M. The tracer was mixed with the chamber water for 10 min, after which a second water sample was withdrawn for the calculation of the $^{15}NO_3^-$ enrichment. The remaining seven water samples were withdrawn at regular intervals. Samples for analysis of the isotopic compositions of N_2 and N_2O were collected in 12 mL Exetainers to which 100 μL of 7 M $ZnCl_2$ were added to stop microbial activity. Samples for analysis of $^{15}NH_4^+$ were filtered through pre-cleaned syringe filters (cellulose acetate, 0.45 μm pore size) and immediately frozen.

Onboard core and slurry incubations

Onboard sediment core incubations were conducted to measure the partitioning of denitrification and DNRA products between water and sediment (De Brabandere et al. 2015). Sediment cores (inner Ø 4.6 cm, $n = 15$) were collected as described for the microsensor measurements. The sediment cores were transferred to a cold room kept at in situ temperature and were placed uncapped in a 25-liter incubation tank filled with bottom water. The water in the tank was purged with a mixture of N_2 and air to maintain in situ O_2 concentrations. Externally driven magnetic stirrers were positioned halfway down the water column of each core, gently stirring the water.

Triplicate water samples from the tank were filtered through pre-cleaned syringe filters (cellulose acetate, 0.45 μm pore size) and frozen for later analysis of nutrients (NH_4^+ and NO_x^-). A 200 mM $^{15}NO_3^-$ solution was added to the water to increase the in situ concentration of NO_3^- by $\sim 70\,\mu$M, after which three more water samples were collected for nutrient analysis. The cores were left in the tank for 1.5–3.5 h to allow for the added $^{15}NO_3^-$ to mix with the endogenous NO_3^- and to establish a linear production of ^{15}N–N_2 (Robertson et al. 2019). After this preincubation, the cores were capped with rubber stoppers and were incubated for 12–16 h. The O_2 concentration was measured in each core with an O_2 sensor spot (OXSP5, Pyro Science) just before capping and after uncapping to ensure that the concentration did not decrease below 30% of the initial value (Dalsgaard et al. 2000). At each time point (directly after capping the cores and every 3–4 h during the incubation) samples were taken from three cores. From each core, a water sample for analysis of the isotopic composition of N_2 and N_2O was transferred to 12 mL Exetainer (Labco Limited) to which 100 μL of 7 M $ZnCl_2$ was added. Another water sample for nutrient and $^{15}NH_4^+$ analysis was filtered (cellulose acetate, 0.45 μm pore size) and frozen. The water and upper 7 cm sediment were then homogenized with a glass rod. A sample for analysis of the isotopic composition of N_2 and N_2O was transferred from the homogenized core to 12 mL Exetainer to which 200 μL of 7 M $ZnCl_2$ were added. One more sample was extracted with Rhizon samplers (Rhizon SMS, Rhizoshpere) and immediately frozen for nutrient and $^{15}NH_4^+$ analysis.

To estimate the relative contribution of anammox to the N_2 production, slurry incubations (Thamdrup and Dalsgaard 2002; Risgaard-Petersen et al. 2003) were conducted at Stas. A and D in 2017. Anammox was assumed to not be active at Stas. E and F, since it was not detected at these sites by Hall et al. (2017) in 2015. Sediment for the slurry incubations was collected with a multiple corer (inner Ø 9.9 cm). The top 1.5 cm from two sediment cores were homogenized and 100 mL of sediment were mixed with 900 mL of filtered (cellulose acetate, 0.45 μm pore size), anoxic bottom water in a glass bottle. The slurry was subsequently bubbled with N_2 for 10 min to remove any O_2 contamination. The slurry was transferred to 12 mL Exetainers (n = 35), each containing a 4-mm glass bead. The samples were left to preincubate on a rotating wheel for about 10 h to remove any residual O_2 and NO_x^-. The slurries were then treated with 150 μL 9 mM deoxygenated solutions of either $^{15}NO_3^-$ ($n = 15$) or $^{15}NH_4^+ + {}^{14}NO_3^-$ ($n = 15$), injected through the vial septa, or were left without additions to serve as controls ($n = 5$). The slurries were incubated on the rotating wheel for 8 h. Directly after addition of the tracers and every 2 h during the incubation, 200 μL of 7 M $ZnCl_2$ were injected to three Exetainers from each treatment and one control to stop the incubation. All operations were conducted at in situ temperature.

Chemical analyses

Solid phase C and N samples were analyzed on an elemental analyzer (Carlo ERBA N1500g, precision $\pm$ 1%). Samples for organic C (OC) were treated with acid fumes (HCl, 37%) to remove carbonate solids before analysis.

Concentrations of NH_4^+ and NO_x^- from the lander chambers were determined by segmented flow colorimetric analysis (Alpkem Flow Solution IV, OI Analytical), using standard

procedures based on those described by Koroleff (1983). The analytical uncertainties were 0.036 μmol N L^{-1} for low (0.036–1.43 μmol N L^{-1}) and 2.4% for high (>1.43 μmol N L^{-1}) concentrations of NH_4^+ and 0.021 μmol N L^{-1} for low (0.014–1.43 μmol N L^{-1}) and 2.5% for high (>1.43 μmol N L^{-1}) concentrations of NO_x^-. DIC concentrations were determined on the ship by infrared detection of CO_2 (LI-6262 CO_2 analyzer, LI-COR) after acidification with phosphoric acid as described by Nilsson et al. (2021). The analytical uncertainty for DIC was 0.2%.

The isotopic compositions of N_2, N_2O, and NH_4^+ were analyzed by coupled gas chromatography–isotope ratio mass spectrometry (GC-IRMS) following the procedure described in De Brabandere et al. (2015). A 2 mL helium (He) headspace was created in the Exetainers, which were then left upside down for 1 day in order for the gases to equilibrate between water and headspace. Subsamples of the headspace were injected to a custom-made GC extraction line coupled to an IRMS (Thermo Delta V Plus). Both N_2 and N_2O were analyzed in the same sample injection whereby N_2 and N_2O were separated in the GC column and any N_2O was reduced to N_2 in a combustion oven (600°C), thus resulting in two temporally separated N_2 peaks. Samples for measurement of $^{15}NH_4^+$ were treated with alkaline hypobromite to oxidize NH_4^+ to N_2 (Warembourg 1993) and were then analyzed as described above.

Calculations and statistics

Sediment–water fluxes were calculated as the change in concentration per unit sediment surface area and time in each chamber following Hylén et al. (2021). Fluxes of O_2 were calculated from linear fits of the chamber O_2 concentration over time. The range of O_2 data used in the calculations was selected as the number of data points during a minimum of 30 min in the initial portion of an incubation that gave the highest r^2 value (typically better than 0.99). For calculation of fluxes from discrete water samples, the concentrations were first corrected for the small dilution of chamber water by ambient water that occurs when a sample is withdrawn. A simple or quadratic linear regression model was then fitted to data of concentration vs. time. Diagnostic graphs of data were used to ensure that the assumptions of linear regression were fulfilled and unusual observations (leverage points and outliers) were removed after identification using Cook's distance values and studentized deleted residual index. The flux was calculated by multiplying the chamber height with the slope of the regression line at the first time point. For about 14% of the fluxes, the slope of the regression model did not significantly differ from 0 ($p > 0.05$). Following a visual inspection of all fluxes, which confirmed that the nonsignificant fluxes did not deviate strongly from the significant fluxes, the nonsignificant (and generally low) fluxes were retained in the data set to avoid underestimation of the average fluxes.

Production rates of ^{15}N-labeled N_2, N_2O, and NH_4^+ were calculated from the slopes of linear regression models fitted to data of excess $^{29,30}N_2$, $^{45,46}N_2O$, and $^{15}NH_4^+$ vs. time. The denitrification rate (N_2 and N_2O production; D_{tot}), and denitrification driven by NO_x^- from the overlying water (D_w) or sedimentary nitrification (D_n), were calculated using the isotope pairing technique (IPT) (Nielsen 1992). If anammox is contributing to the N_2 production, rates must be calculated using the revised IPT (Risgaard-Petersen et al. 2003). However, no anammox was found (*see* Results section), so denitrification rates were calculated using the classical IPT. DNRA rates ($DNRA_{tot}$) and DNRA driven by NO_x^- from the overlying water ($DNRA_w$) or sedimentary nitrification ($DNRA_n$) were calculated according to Risgaard-Petersen and Rysgaard (1995). The fractions of denitrification and DNRA that were driven by NO_x^- from sedimentary nitrification were equally large. Hence, both fractions are presented as nitrification – NO_x^- reduction (% NO_x^- red$_n$), calculated as:

$$\%NO_x^- \text{red}n = \frac{D_n}{D_{tot}} \times 100 = \frac{DNRA_n}{DNRA_{tot}} \times 100.$$

As the chambers of the lander only captures the N_2, N_2O, and NH_4^+ that diffuse to the water column (De Brabandere et al. 2015), total denitrification and DNRA rates in the sediment incubated by the chambers of the lander were calculated as follows:

$$R_{tot} = R_{W-lan} \times (R_C/R_W),$$

where $R_{W\text{-lan}}$ is the rate in the water column of the lander chamber, while R_C and R_W are the rates in the homogenized sediment core phase (i.e., sediment and water) and water phase alone, respectively. It was assumed that the partitioning of the added $^{15}NO_3^-$ between water and sediment was the same in the lander chambers and sediment cores.

Data from the in situ incubations were used to calculate correlations between environmental parameters (bottom water O_2 and NO_x^-, sedimentary O_2 uptake and DIC release) and NO_x^- reduction rates. Calculations were done in R (v. 4.0.2; R Core Team 2020). Since Shapiro–Wilk tests (shapiro.test, "stats" v. 4.0.2) showed that some data were not normally distributed, Spearman's rank correlation coefficient was used (corr. test, "psych" v. 2.0.7; Revelle 2020). Correlations with p values <0.05 were considered significant. Due to the low number (≤ 7) of complete data pairs per station and year, correlations were not calculated for sediment parameters (e.g., OC), bottom water salinity and bottom water temperature.

Results

Bottom water conditions and sediment properties

The bottom water at Sta. A was fully oxygenated (100–355 μM O_2) with low NO_x^- concentrations (2.9–8.6 μM; Table 1). In 2017, a storm between two lander deployments caused the halocline to move downward which in turn

increased the O_2 concentration substantially (Table 1; van de Velde et al. 2020), whereas the NO_x^- concentrations did not change. The sediment at Sta. A was generally characterized by three distinct layers: a rust-colored layer down to 2 cm depth, a light-brown layer between 2 and 4 cm depth, followed by post-glacial clay. The OC and N contents in the top 2 cm of sediment were low (0–5% and 0–1%, respectively) but showed some variability between samplings (Table 1; Supporting Information Fig. S1), suggesting spatial heterogeneity. The heterogeneity was also reflected in the OC : N ratios, which varied between 7.0 and 10.5. During the 2018 sampling, we occasionally retrieved sediment of a different type to that which is generally found at the station, finer sediment with darker layers and a deeper post-glacial clay horizon. Animals (polychaetes, isopods and bivalves) were found in the sediment during all samplings.

At Stas. D–F, the sediment was clearly laminated and there were no signs of animal activity. Bottom water concentrations of O_2 and NO_x^- were highest immediately after the inflow, after which they decreased rapidly (Table 1). The OC and N contents in the top 2 cm of sediment were relatively high (7.9–12.1% and 0.9–1.4%, respectively) and the OC : N ratios varied between 9.4 and 10.9. Mats of large filamentous sulfur bacteria were visible on the sediment surface at Sta. D in 2018 and Stas. E and F in 2017 and 2018.

At Sta. A, the O_2 penetration depth (OPD) was approximately 5 mm and H_2S was below the detection limit of the sensor (1 μM) in the top 10 mm, with the exception of one profile in 2015 (Fig. 2). In 2018, we measured decreasing N_2O concentrations from the sediment surface (0.02 μM) to 5 mm depth, where the concentration stabilized at zero. The N_2O concentration at Sta. A was an order of magnitude lower than

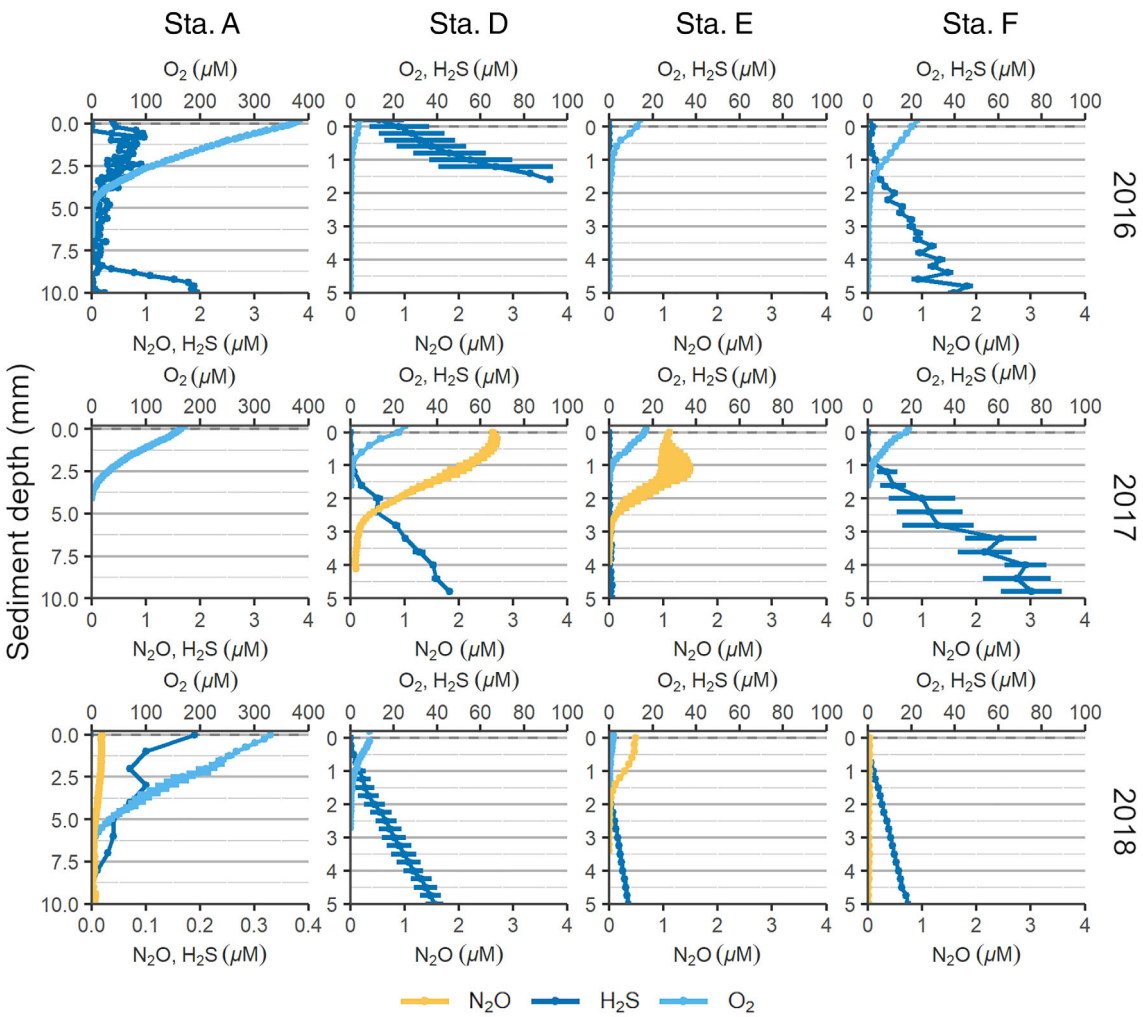

Fig. 2. Sediment microprofiles. Note different scales of the *y*-axes on Sta. A compared to Stas. D–F, and the N_2O/H_2S axes for Sta. A in different years and compared to D–F. profiles of O_2 and H_2S in 2016 and 2017 are from Marzocchi et al. (2018), all profiles in 2018 are from Broman et al. (2020). Error bars show standard errors.

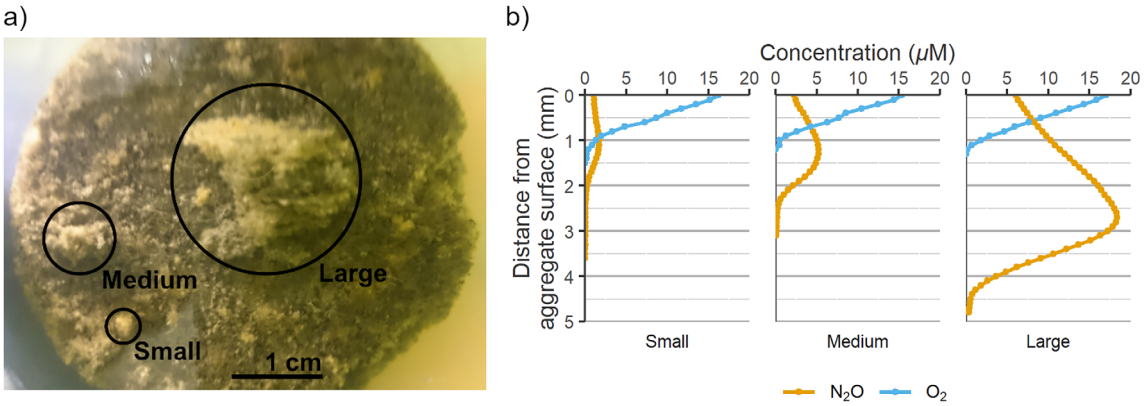

Fig. 3. Aggregate microprofiles from Sta. E. (**a**) Photograph of the profiled aggregates. (**b**) Microprofiles of N_2O and O_2. Zero on the *y*-axes refers to the aggregate surface.

at Stas. D and E. Conversely, the OPDs were substantially lower at Stas. D, E and F than at Sta. A, ranging between 0.7 mm at Sta. E in 2018 and 2.1 mm at Sta. F in 2016. At these newly oxygenated stations, the microsensors showed higher bottom water O_2 concentrations than the optodes on the lander, likely due to O_2 contamination in the ex situ core incubations (Table 1, Fig. 2; Marzocchi et al. 2018a,b). At Stas. D and F, H_2S appeared between the surface and 1 mm depth, whereas it was not detected until 2 mm or deeper at Sta. E. Peaks of N_2O were visible in zones with little (< 15 μM) or no O_2 at Stas. D and E. The N_2O concentrations reached 3 μM at these stations in 2017, while they were around 0 μM at Sta. F and < 0.5 μM at Sta. E in 2018 (Broman et al. 2020).

The OPDs in all three aggregates from Sta. E were about 1 mm (Fig. 3). Peaks of N_2O were present in the anoxic part of all aggregates, with increasing concentrations and deepening peaks with increasing aggregate size. The N_2O concentrations in the aggregates ranged from values similar to, to one order of magnitude higher, than in the sediment at Sta. E (Figs. 2, 3d).

Pore-water profiles (Supporting Information Fig. S2) of NH_4^+ at Sta. A showed a peak of 70 μM at 2 cm depth. The profiles stabilized at ~40 μM below 5 cm depth, around the depth where post-glacial clay started to occur. At Stas. D–F, the profiles increased from about 50 μM at the sediment surface to 150–250 μM at 20 cm depth. The NO_x^- profiles at Sta. A displayed multiple peaks between the surface and 5 cm depth, suggesting that bioturbation was bringing O_2 to deeper sediment layers, thereby enabling nitrification. No NO_x^- peaks were detected in the sediment at Stas. D–F. It is likely that the resolution of the pore-water profiles was too low to show any production of NO_x^- at these stations, as the top sediment slice was 5 mm thick while the OPD (and thereby the potential nitrification zone) was less than 2 mm.

Benthic fluxes

Compared to 2016 and 2017, the fluxes of O_2 and DIC at Sta. A were twice as high in 2018, and low NO_x^- effluxes or even NO_x^- uptake were measured (Fig. 4). That year, the incubation at Sta. A likely took place at more reactive sediment, as suggested by the finer and likely more organic matter-rich sediment with darker layers (*see* "Sediment properties and microsensor measurements" section). The O_2 uptake (4–19 mmol m^{-2} d^{-1}) were in the same range as the DIC efflux (6–12 mmol m^{-2} d^{-1}). The fluxes of NH_4^+ and NO_x^- were low (< 0.3 mmol m^{-2} d^{-1}) and on average directed out of the sediment.

Fluxes of DIC and dissolved inorganic nitrogen (NH_4^+ + NO_x^-) at Stas. D–F were presented by Hylén et al. (2021). At these deeper stations, fluxes of O_2 were only measurable the year following inflows (2017 at Sta. D, 2016 at Stas. E and F; Fig. 4). The fluxes of DIC (24–76 mmol m^{-2} d^{-1}) and NH_4^+ (2–8 mmol m^{-2} d^{-1}) were substantially higher than at the shallow station. During the years when NO_x^- was available in the water column, it was taken up by the sediment at rates up to ~1 mmol m^{-2} d^{-1}.

NO_x^- reduction rates

Denitrification and DNRA rates were measured at all sites, no anammox was detected. Denitrification was the only measurable process at Sta. A in 2017, with a rate of 40 μmol m^{-2} d^{-1} (Fig. 5a). In 2018, the denitrification rate had increased 18-fold (to 755 μmol m^{-2} d^{-1}) and DNRA (60 μmol m^{-2} d^{-1}) was detected, likely due to the more reactive sediment. Thus, complete denitrification was the dominant NO_3^- reduction process both years (Fig. 5a–c) and sedimentary nitrification was the main source (>80%) of NO_x^- for denitrification and DNRA at Sta. A (Fig. 5d). Values of R_C/R_W at Sta. A were 1.2 for denitrification and 2.9 for DNRA.

The in situ incubations at Sta. D in 2016 (before oxygenation) did not show any $^{29}N_2$ production (data not shown), indicating that reduction of ambient NO_x^- was not active and only a potential denitrification rate (D_{15}) could be calculated. However, production of $^{30}N_2$ and $^{15}NH_4^+$ demonstrated that there was a potential for NO_x^- reduction at the station

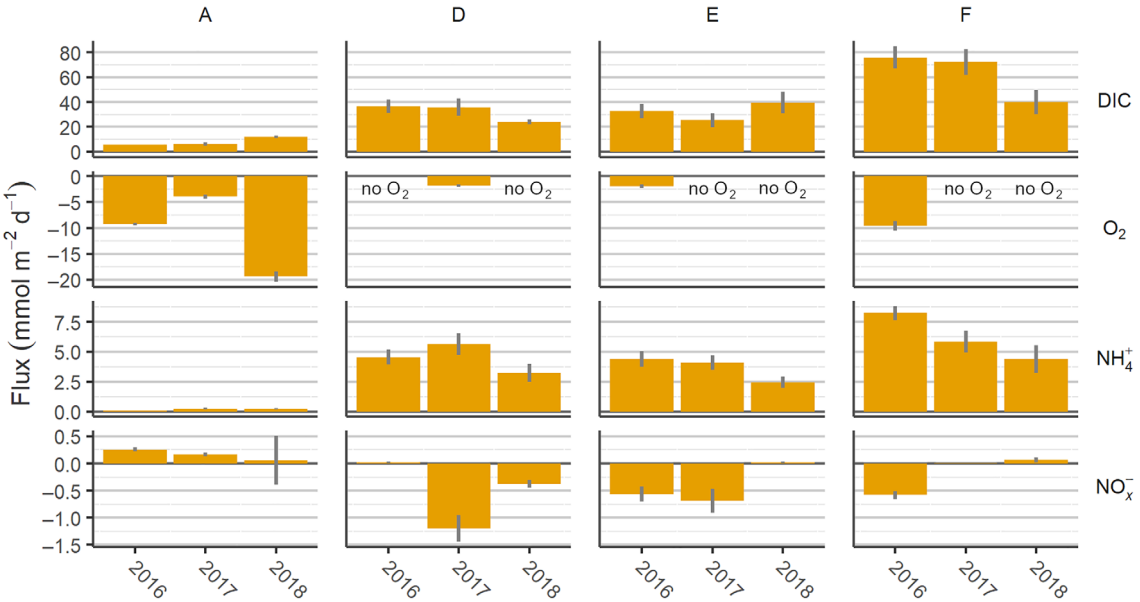

Fig. 4. Sediment–water solute fluxes measured in situ with the benthic chamber lander. Columns show average values, error bars show standard errors. Positive fluxes are directed out of the sediment whereas negative fluxes are sediment uptake. Fluxes of DIC and dissolved inorganic nitrogen (NH_4^+ + NO_x^-) at Stas. D–F from Hylén et al. (2021).

(Supporting Information Table S1). Following oxygenation of Stas. D–F, denitrification (37–112 μmol m^{-2} d^{-1}) and DNRA (33–71 μmol m^{-2} d^{-1}) were detected, with the latter process contributing 31–56% to the total NO_x^- reduction (% DNRA; Fig. 5a,c). The fraction of denitrification that resulted in N_2O production (% N_2O) was 41–88% of the total denitrification and did not change substantially between samplings (Fig. 5a,d). Compared to Sta. A, a much smaller fraction (0–63%) of the NO_x^- reduction was driven by nitrification (Fig. 5d). Values of R_C/R_W at Stas. D–F were 1.5 for denitrification and 1.4 for DNRA.

The denitrification rates correlated negatively with the DIC fluxes and DNRA rates did not correlate with any environmental parameters (Table 2; Supporting Information Fig. S3). However, both % DNRA and % N_2O correlated positively with DIC fluxes and bottom water concentrations of NO_x^-, and negatively with bottom water O_2 concentrations and sedimentary O_2 uptake. The % NO_x^- red$_n$ correlated positively with both bottom water O_2 concentrations and sedimentary O_2 uptake, whereas there was a negative correlation with bottom water concentrations of NO_x^-.

Discussion

Production of N_2O and NH_4^+ dominated after oxygenation

Although benthic NO_x^- reduction was initiated at the previously long-term anoxic stations after the MBI, incomplete denitrification (N_2O production) and DNRA dominated while removal of bioavailable N through N_2 production was of minor importance. Compared to fluxes measured during anoxia in 2008 and 2010 (Hall et al. 2017; Hylén et al. 2021), the efflux of NH_4^+ actually increased at Stas. E and F during the 2 yr after the inflow (Sta. E from 0.6–1.7 to 2.5–4.4 mmol m^{-2} d^{-1} and Sta. F from 3.0–3.2 to 4.4–8.3 mmol m^{-2} d^{-1}; Fig. 4). Similar patterns were also seen for other biogenic compounds (DIC, dissolved silicate, dissolved inorganic phosphorus), suggesting that the degradation of organic matter increased temporarily after the inflow and amplified the NH_4^+ release (Hylén et al. 2021). Overall, the NH_4^+ effluxes were one order of magnitude higher than the NO_x^- reduction rates at the newly oxygenated stations. Thus, while the MBI and resulting oxygenation did lead to some removal of fixed N, the main effect was stimulated N recycling via organic matter mineralization.

The negative correlation between bottom water O_2 concentrations and % DNRA found in this study has also been observed in other parts of the Baltic Sea (the Gulf of Finland and the southern Baltic Proper; Jäntti and Hietanen 2012). Sediments underlying bottom water with little or no O_2 are generally more reduced, which is considered to favor DNRA (*see* "Strongly reduced sediments favor DNRA" section). The extent of the oxygenation is also likely to have an effect on the partitioning between NO_x^- reduction processes. There was a decrease in % DNRA with increasing O_2 exposure time during artificial oxygenation of the By Fjord on the west coast of Sweden (from ~65% to ~45% in 2 yr; De Brabandere et al. 2015). In our study, however, no clear change in either rates or % DNRA with time was observed over the few consecutive samplings (Fig. 5a,c). This discrepancy in response can likely be explained by different degrees of oxygenation between the two studies. The bottom water O_2 concentration in the By Fjord

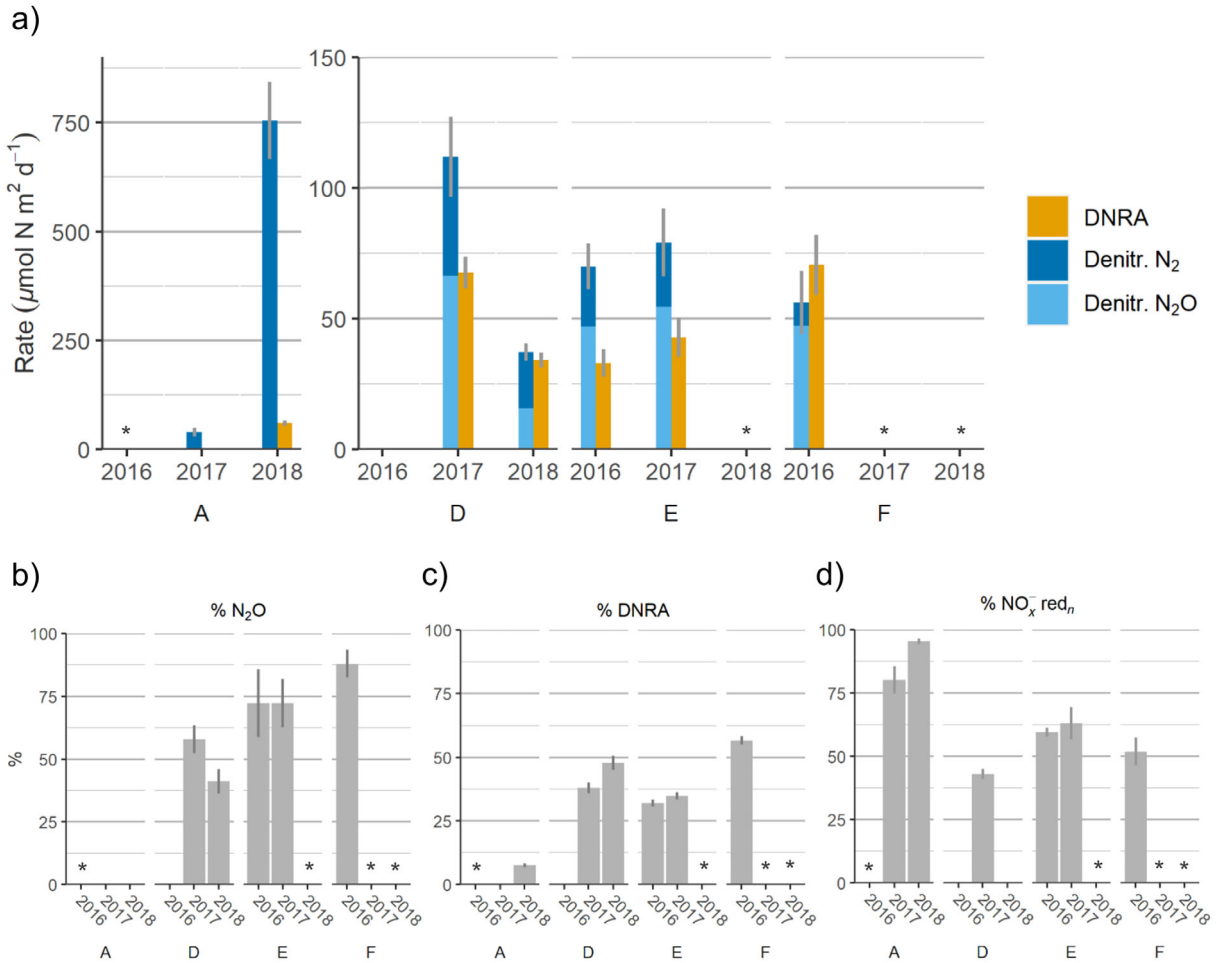

Fig. 5. NO_x^- reduction rates measured with the Gothenburg benthic chamber landers. (**a**) Rates of DNRA and denitrification (N_2 and N_2O production). (**b**) Fraction of denitrification ending with N_2O. (**c**) Fraction of DNRA of the total NO_x^- reduction. (**d**) Fraction of NO_x^- reduction driven by NO_x^- from sedimentary nitrification. Asterisk indicates no measurement (*see* Table 1).

was continuously 40–140 μM following oxygenation and the OPD increased with time, suggesting that the sediment was gradually becoming less reduced (De Brabandere et al. 2015). In the Eastern Gotland Basin, the natural oxygenation of the bottom water was likely too weak and not constant enough (< 50 μM O_2, Table 1; Fig. 1; Hall et al. 2017) to change the sediment geochemistry sufficiently for a shift in the balance between denitrification and DNRA to occur.

The bottom water O_2 concentration also correlated negatively with % N_2O (Table 2). This correlation, however, as well as those with bottom water NO_x^- concentrations and O_2 uptake, was driven by the large differences between Stas. A

Table 2. Spearman's rank correlation coefficient for correlations between NO_x^- reduction rates and environmental parameters. Correlations marked in bold were statistically significant.

	BW O_2	BW NO_X^-	Sed. O_2 uptake	Sed. DIC release
Denitr.	0.31	−0.35	0.33	**−0.46***
DNRA	0.13	0.09	0.13	−0.05
% NO_x^- red$_n$	**0.71*****	**−0.52****	**0.71*****	−0.25
% N_2O	**−0.49***	**0.65*****	**−0.48***	**0.69*****
% DNRA	**−0.51****	**0.61*****	**−0.52****	**0.47***

*$p < 0.05$; **$p < 0.01$; ***$p < 0.001$.

and D–F rather than showing a trend over all stations (Supporting Information Fig. S3). Bottom water O_2 concentrations were thus unlikely to have been a major driver behind % N_2O patterns at the newly oxygenated stations. Instead, the last step in the denitrification process was likely inhibited by H_2S (Sørensen et al. 1980; Senga et al. 2006) at Stas. D–F, which reached the sedimentary NO_x^- reduction zone at these newly oxygenated stations (Fig. 2). No net production of N_2O through denitrification was detected at Sta. A as determined from ^{15}N isotope incubations (Fig. 5), in agreement with previous studies of permanently oxic sites in the Baltic Sea (Hellemann et al. 2017, 2020; Bartl et al. 2019). A small N_2O peak was visible in the oxic part of the sediment in 2018 (Fig. 2), suggesting production through nitrification. The microprofiles suggest that little to no of this N_2O was released from the sediment at Sta. A, however.

Interestingly, microprofiling of individual aggregates deposited on the seafloor at Sta. E showed that they were sites of production of N_2O (Fig. 3b). The N_2O production peaks were located in the anoxic parts of the aggregates, suggesting that denitrification was the responsible process. Aggregates can form as phytoplankton sink from the surface (Thornton 2002), and also as fresh and reactive organic matter is resuspended and transported from shallow to deeper areas in the Eastern Gotland Basin (Nilsson et al. 2021). Aggregates are locations of high degradation of organic matter and thereby form anoxic microniches with intense N cycling, both while sinking and once settled on the seafloor (Klawonn et al. 2015; Bianchi et al. 2018; Marzocchi et al. 2018b). The positive correlation observed between % N_2O and the DIC fluxes further suggests a connection between N_2O production and hot spots of organic matter degradation. These hot spots could occur in the sediment due to local heterogeneities, but also in aggregates consisting of fresh organic matter.

Strongly reduced sediments favor DNRA

The contribution from DNRA to the total NO_x^- reduction rates is generally found to be higher in active, more reduced systems with high concentrations of organic matter (Giblin et al. 2013; Kessler et al. 2018). This trend is often attributed to the ratio between NO_x^- and electron donors (e.g., OC and H_2S). Although denitrification yields more energy per mole of electron donor, more electrons are transferred per mole of NO_x^- during DNRA (Tiedje et al. 1983). As such, DNRA tends to be favored in environments with high availability of electron donors relative to NO_x^- (Kraft et al. 2014; Hardison et al. 2015; van den Berg et al. 2015).

The positive correlation between % DNRA and the bottom water NO_x^- concentrations observed in this study (Table 2; Supporting Information Fig. S3) seems to contradict the theory that DNRA dominates under lower NO_x^- conditions. However, the ratio between NO_x^- and electron donors differed substantially between the permanently oxic Sta. A and the newly oxygenated Stas. D–F. Although the bottom water NO_x^- concentrations generally were lower at Sta. A than at Stas. D–F during years of oxygenation, the OC content in the sediment was one order of magnitude higher at Stas. D–F than at Sta. A (Table 1) and H_2S was present < 2 mm from the surface at the former sites (Fig. 2; Marzocchi et al. 2018a). The ratios between bottom water NO_x^- and these potential electron donors were thus substantially higher at Sta. A than at Stas. D–F, which likely contributed to the observed partitioning between processes. The positive correlation between DIC fluxes and % DNRA, and negative correlation between DIC fluxes and denitrification rates, further suggested that DNRA was favored at sites with high organic matter degradation. It is also possible that % DNRA changed over the year. The sampling for this study was conducted right before the spring bloom each year (Hylén et al. 2021). The importance of DNRA could therefore have grown in the months after the samplings, as the spring bloom was deposited on the sediment and increased the supply of reactive organic matter, for example, in the form of aggregates.

Whereas sediment denitrification generally is heterotrophic (Seitzinger et al. 2006), we cannot conclusively say which electron donor (OC or H_2S) that was used in DNRA. Nevertheless, detection of sulfur bacteria (cable bacteria and *Beggiatoa* spp.) able to mediate DNRA in the sediment from the Eastern Gotland Basin (Yücel et al. 2017; Marzocchi et al. 2018a, 2021) suggests that a fraction of DNRA was coupled to H_2S oxidation. Furthermore, it has recently become clear that Fe^{2+} also can be an important electron donor for DNRA (Robertson et al. 2016; Kessler et al. 2018). Low concentrations (< 10 μM) of Fe^{2+} appeared in the pore water at Stas. D–F after the MBI, as iron oxides that had formed in the water column sank and were reductively dissolved in the sediment (van de Velde et al. 2020). However, the concentrations of Fe^{2+} were one order of magnitude lower than at sites where it has been shown to enhance DNRA (Robertson et al. 2016) and the Fe^{2+} concentrations in the sediment at Stas. D–F were considerably lower than those of OC and H_2S. We thus consider it unlikely that Fe^{2+} was an important electron donor for DNRA in this system or played a significant role in the partitioning between denitrification and DNRA.

While both denitrification and DNRA were important at Stas. D–F, denitrification dominated at Sta. A. The NO_x^- reduction rates at Sta. A varied substantially between years but were comparable to previous measurements from well-oxygenated sites with low sedimentary OC content in the Baltic Sea (Jäntti and Hietanen 2012; Bonaglia et al. 2017; Hellemann et al. 2020). The large difference in rates between years was likely caused by spatial heterogeneity at Sta. A, as explained above, resulting in incubation of more reactive sediment in lander chambers in 2018. The layered and darker appearance of the sediment in 2018 compared to 2016–2017, in combination with high DIC and O_2 fluxes, suggest that the location was richer in OC and that the mineralization rates were higher. Since the bottom water at Sta. A was well-oxygenated

with low NO_x^- concentrations, a higher sedimentary OC content would likely have stimulated denitrification, as reported from other sites in the Baltic Sea (Jäntti et al. 2011; Bartl et al. 2019).

In contrast to some relatively organic matter-poor (2.5–5.1% OC) sites in the Baltic Sea where anammox constituted 5–32% of the NO_x^- reduction (Bonaglia et al. 2014, 2017; van Helmond et al. 2020), the process was insignificant at Sta. A. Although the sedimentary OC content is low at the site, the material is readily degraded compared to other areas of the Baltic Sea (Nilsson et al. 2021). Compared to sites where anammox has been shown to significantly contribute to NO_x^- reduction, it is possible that the available OC at Sta. A was reactive enough that heterotrophic denitrification would outcompete anammox (Devol 2015).

NO_x^- limited denitrification and DNRA

The potential NO_x^- reduction rates (D_{15}, Supporting Information Table S1) measured at Sta. D in 2016, before introduction of O_2 and NO_x^-, suggest that microorganisms capable of NO_x^- reduction were present in the sediment at the time of the MBI. Sta. D experiences minor inflows more regularly than Stas. E and F (Supporting Information Fig. S5; SMHI 2021) and is more likely to maintain active NO_x^- reduction metabolisms. Potential for NO_x^- reduction has been previously measured in long-term anoxic sediments (De Brabandere et al. 2015). Thus, as have been seen at other sites, NO_x^- reducing activity was rapidly resumed in the sediments of Stas. D–F as NO_x^- became available after the MBI, even after a prolonged period of NO_x^--free bottom water.

The denitrification and DNRA rates at Stas. D–F were in the lower range of rates measured in the Baltic Sea at sites with low bottom water O_2 concentrations and high sedimentary OC content (Bonaglia et al. 2014; Hellemann et al. 2020). A likely reason for the low rates is NO_x^- limitation. Nitrification was not measured in this study, but substantial sedimentary NH_4^+ effluxes (Fig. 4) and relatively low bottom water NO_x^- concentrations (Table 1) suggest that the process was inhibited at Stas. D–F. This could be the result of restrictions caused by the very narrow horizon of oxygenated sediment where nitrification could occur, potentially in combination with inhibition of nitrification by H_2S (Joye and Hollibaugh 1995). Denitrification and DNRA rates were indeed slightly higher directly after the inflow in 2015 (50–160 and 160–530 μmol m^{-2} d^{-1}, respectively), when bottom water O_2 concentrations were higher (Hall et al. 2017).

Sedimentary nitrification contributed half of the NO_x^- being reduced at Stas. D–F (Fig. 5d), despite shallow OPDs (1–2.2 mm, Fig. 2). The only exception was Sta. D in 2018, where anoxia had returned and the water column was the only source of NO_x^- for reduction. The highest % NO_x^- red$_n$ (>75%) was measured at the permanently oxic Sta. A, where the OPD was consistently deeper (4–7 mm) than at Stas. D–F and porewater NO_x^- profiles (Supporting Information Fig. S2) suggest that bioturbation enabled nitrification further down in the sediment. Higher bottom water O_2 concentrations tend to increase the importance of NO_x^- red$_n$ since deeper O_2 penetration pushes the zone of nitrification further down into the sediment, which decreases the diffusional loss of NO_x^- to the water column (Rysgaard et al. 1994). The positive correlation between % NO_x^- red$_n$ and bottom water O_2 concentration (Table 2) suggest that this was indeed occurring at our sites. On the other hand, high bottom water concentrations of NO_x^- can decrease the relative importance of NO_x^- red$_n$, as diffusion of water column NO_x^- into the sediment increases (Rysgaard et al. 1994; Seitzinger et al. 2006; De Brabandere et al. 2015). In agreement with this theory, we also saw a negative correlation between % NO_x^- red$_n$ and bottom water NO_x^- concentrations (Table 2).

Interestingly, the sedimentary uptake of NO_x^- was ~5–7 times higher than the NO_x^- reduction rates at Stas. D–F. A plausible explanation for this excess uptake is intracellular NO_x^- storage by organisms such as large sulfur bacteria, diatoms, and foraminifera (McHatton et al. 1996; Kamp et al. 2015). Mats of the large sulfur bacteria *Beggiatoa* spp. were visible on the sediment surface in 2017 and 2018. Members of the Beggiatoaceae family use O_2 and NO_x^- to oxidize H_2S, and are capable of storing NO_x^- at concentrations over 100 μM in their vacuoles (McHatton et al. 1996). These bacteria are known to perform both denitrification and DNRA, but DNRA is believed to be the dominant pathway in sulfide-rich sediments (Schutte et al. 2018).

The presence of organisms with intracellular NO_x^- storage can cause two main issues that may compromise the IPT unless additional experiments are carried out (Robertson et al. 2019). First, since the added $^{15}NO_3^-$ is unlikely to equilibrate with the intracellular pools of NO_x^-, the reduction of $^{14}NO_x^-$ from intracellular pools would not be captured by the IPT and the total NO_x^- reduction rate would be underestimated. Second, the combination of added $^{15}NO_3^-$ and $^{14}NO_x^-$ from intracellular pools during denitrification would give an increased production of $^{29}N_2$, which would be mistaken as NO_x^- red$_n$. The NO_x^- reduction rates presented here should therefore be seen as a lower limit as the true amount of NO_x^- reduction from intracellular NO_x^- and water column-derived NO_x^- may be underestimated in our calculations.

Conclusions and environmental implications

Sedimentary NO_x^- reduction was stimulated in the Eastern Gotland Basin after the MBI, however, we demonstrate that these processes had only a small impact on the capacity to remove N as N_2 through denitrification at the newly oxygenated sites. The weak and inconsistent oxygenation combined with high sedimentary production of reduced species (e.g., H_2S) likely limited nitrification, and thus nitrification–denitrification. Due to the high NH_4^+ release and low denitrification rates, the denitrification efficiency (N_2,N_2O-N/[N_2,N_2O-N

+ fluxes of NH_4^+ and NO_x^-] × 100%; Eyre and Ferguson 2009) was only 0.7–2.4% at Stas. D–F, compared to 9.1–72.5% at Sta. A. Denitrification rates at the newly oxygenated stations were in the lower range of measurements at similar sites in the Baltic Sea (Bonaglia et al. 2014; Hellemann et al. 2020) and also in the lower range of denitrification rates at the oxic–anoxic interface in the water column of the Eastern Gotland Basin (60–211 μmol N m^{-2} d^{-1}; Dalsgaard et al. 2013). As the MBI and following inflows created a second oxic–anoxic interface in the water column, the pelagic N removal is likely to have increased considerably, substantially exceeding the sedimentary N removal (Hall et al. 2017). In conclusion, the sediment at the newly oxygenated stations was not sites of efficient removal of fixed N. The natural oxygenation event stimulated production of N_2O and recycling of fixed N through DNRA, while increased organic matter degradation lead to elevated release of fixed N as NH_4^+ (Hylén et al. 2021). Consequently, the main outcome from this temporary oxygenation was that the sediments continued to contribute to accumulation, rather than removal, of fixed N in the system.

Our results showing dominance of denitrification at the site with less organic matter (A) and a substantial contribution from DNRA at the hypoxic sites with organic rich and reduced sediments (D–F) follow patterns observed in the Baltic Sea (Jäntti and Hietanen 2012; Bonaglia et al. 2017; van Helmond et al. 2020) and elsewhere (e.g., estuaries in Victoria, Australia, Kessler et al. 2018; the By Fjord, Sweden, De Brabandere et al. 2015; sediments below the Peruvian O_2 minimum zone, Bohlen et al. 2011). The high proportion of N_2O production from incomplete denitrification, however, was unexpected. While N_2O released from the sediment at Stas. D–F was likely oxidized in the water column (Myllykangas et al. 2017; Broman et al. 2020), a similar release in shallower areas with hypoxic bottom waters could potentially reach the atmosphere. As O_2-depleted zones are expanding in coastal areas (Altieri and Gedan 2015), the exact mechanisms behind increased N_2O production observed under fluctuating oxygen conditions (this study; Myllykangas et al. 2017; Broman et al. 2020) deserve attention in future studies. Shallowing of O_2-depleted zones could have an even stronger effect on the sedimentary N_2O release if aggregates are important sites of N_2O production, as suggested by our measurements. In shallow areas, a larger fraction of sinking aggregates escapes degradation in the water column. A higher deposition of relatively more labile aggregates may stimulate N_2O production at shallow sites where the severity and persistence of low-O_2 bottom waters is increasing. The shorter transport distance from sediments to surface waters may thus result in an increased N_2O release to the atmosphere in O_2-depleted coastal zones, thereby intensifying global warming.

The spreading of oxygen-depleted zones in coastal areas around the world has led to a growing interest in the response of the benthic N cycle to hypoxia (De Brabandere et al. 2015; Song et al. 2020). Studies have shown varying results depending on local environmental conditions, but there is a tendency toward decreased removal of fixed N under severe hypoxia and anoxia (Jäntti and Hietanen 2012; Caffrey et al. 2019; Song et al. 2020). These studies generally focus on seasonally hypoxic areas, however. Here, we expand the studied areas to include long-term anoxic (euxinic) sediments that have been affected by eutrophication for decades (Carstensen et al. 2014). Our observations suggest that transient oxygenation of these strongly reduced systems may not lead to efficient sedimentary removal of fixed N, and instead the sedimentary release of reduced N compounds can accelerate the return to the original anoxic state.

Data availability statement

Upon publication, all data included in this manuscript will be available to download from the Swedish National Data Service.

References

Altieri, A. H., and K. B. Gedan. 2015. Climate change and dead zones. Glob. Chang. Biol. **21**: 1395–1406. doi:10.1111/gcb.12754

Andersen, K., T. Kjær, and N. P. Revsbech. 2001. An oxygen insensitive microsensor for nitrous oxide. Sens. Actuators B **81**: 42–48. doi:10.1016/S0925-4005(01)00924-8

Bartl, I., D. Hellemann, C. Rabouille, K. Schulz, P. Tallberg, S. Hietanen, and M. Voss. 2019. Particulate organic matter controls benthic microbial N retention and N removal in contrasting estuaries of the Baltic Sea. Biogeosciences **16**: 3543–3564. doi:10.5194/bg-16-3543-2019

Beusen, A. H. W., A. F. Bouwman, L. P. H. Van Beek, J. M. Mogollón, and J. J. Middelburg. 2016. Global riverine N and P transport to ocean increased during the 20th century despite increased retention along the aquatic continuum. Biogeosciences **13**: 2441–2451. doi:10.5194/bg-13-2441-2016

Bianchi, D., T. S. Weber, R. Kiko, and C. Deutsch. 2018. Global niche of marine anaerobic metabolisms expanded by particle microenvironments. Nat. Geosci. **11**: 1–6. doi:10.1038/s41561-018-0081-0

Blomqvist, S., N. Ekeroth, R. Elmgren, and P. O. J. Hall. 2015. Long overdue improvement of box corer sampling. Mar. Ecol. Prog. Ser. **538**: 13–21. doi:10.3354/meps11405

Bohlen, L., A. W. Dale, S. Sommer, T. Mosch, C. Hensen, A. Noffke, F. Scholz, and K. Wallmann. 2011. Benthic nitrogen cycling traversing the Peruvian oxygen minimum zone. Geochim. Cosmochim. Acta **75**: 6094–6111. doi:10.1016/j.gca.2011.08.010

Bonaglia, S., B. Deutsch, M. Bartoli, H. K. Marchant, and V. Brüchert. 2014. Seasonal oxygen, nitrogen and phosphorus benthic cycling along an impacted Baltic Sea estuary: Regulation and spatial patterns. Biogeochemistry **119**: 139–160. doi:10.1007/s10533-014-9953-6

Bonaglia, S., and others. 2017. The fate of fixed nitrogen in marine sediments with low organic loading: An in situ study. Biogeosciences **14**: 285–300. doi:10.5194/bg-14-285-2017

Breitburg, D. L., L. A. Levin, A. Oschlies, and others. 2018. Declining oxygen in the global ocean and coastal waters. Science **359**: 1–11. doi:10.1126/science.aam7240

Broman, E., S. Bonaglia, O. Holovachov, U. Marzocchi, P. O. J. Hall, and F. J. A. Nascimento. 2020. Uncovering diversity and metabolic spectrum of animals in dead zone sediments. Commun. Biol. **3**: 1–12. doi:10.1038/s42003-020-0822-7

Caffrey, J. M., S. Bonaglia, and D. J. Conley. 2019. Short exposure to oxygen and sulfide alter nitrification, denitrification, and DNRA activity in seasonally hypoxic estuarine sediments. FEMS Microbiol. Lett. **366**: 1–10. doi:10.1093/femsle/fny288/5266299

Canfield, D. E., E. Kristensen, and B. Thamdrup. 2005. Aquatic geomicrobiology. Elsevier Academic Press.

Carstensen, J., J. H. Andersen, B. G. Gustafsson, and D. J. Conley. 2014. Deoxygenation of the Baltic Sea during the last century. Proc. Natl. Acad. Sci. **111**: 5628–5633. doi:10.1073/pnas.1323156111

Dalsgaard, T., and F. Bak. 1994. Nitrate reduction in a sulfate-reducing bacterium, *Desulfovibrio desulfuricans*, isolated from rice paddy soil: Sulfide inhibition, kinetics, and regulation. Appl. Environ. Microbiol. **60**: 291–297. doi:10.1128/aem.60.1.291-297.1994

Dalsgaard, T., and others. 2000. Protocol handbook for NICE—nitrogen cycling in estuaries: A project under the EU research programme. Marine Science and Technology (MAST III), National Environmental Research Institute.

Dalsgaard, T., L. De Brabandere, and P. O. J. Hall. 2013. Denitrification in the water column of the Central Baltic Sea. Geochim. Cosmochim. Acta **106**: 247–260. doi:10.1128/mBio.01966-14

De Brabandere, L., S. Bonaglia, M. Y. Kononets, L. Viktorsson, A. Stigebrandt, B. Thamdrup, and P. O. J. Hall. 2015. Oxygenation of an anoxic fjord basin strongly stimulates benthic denitrification and DNRA. Biogeochemistry **126**: 131–152. doi:10.1007/s10533-015-0148-6

Devol, A. H. 2015. Denitrification, anammox, and N_2 production in marine sediments. Ann. Rev. Mar. Sci. **7**: 403.

Diaz, R. J., and R. Rosenberg. 2008. Spreading dead zones and consequences for marine ecosystems. Science **321**: 926–929. doi:10.1126/science.1156401

Eyre, B. D., and A. J. P. Ferguson. 2009. Denitrification efficiency for defining critical loads of carbon in shallow coastal ecosystems, p. 137–146. *In* J. H. Andersen and D. J. Conley [eds.], Eutrophication in coastal ecosystems: Towards better understanding and management strategies. Springer.

Fossing, H., and others. 1995. Concentration and transport of nitrate by the mat-forming sulphur bacterium *Thioploca*. Nature **374**: 713–715. doi:10.1038/374713a0

Galloway, J. N., and others. 2008. Transformation of the nitrogen cycle: Recent trends, questions, and potential solutions. Science **320**: 889–892. doi:10.1126/science.1136674

Giblin, A. E., C. Tobias, B. Song, N. Weston, G. Banta, and V. Rivera-Monroy. 2013. The importance of dissimilatory nitrate reduction to ammonium (DNRA) in the nitrogen cycle of coastal ecosystems. Oceanography **26**: 124–131. doi:10.5670/oceanog.2013.54

Hall, P. O. J., and others. 2017. Influence of natural oxygenation of Baltic proper deep water on benthic recycling and removal of phosphorus, nitrogen, silicon and carbon. Front. Mar. Sci. **4**: 1–14. doi:10.3389/fmars.2017.00027

Hardison, A. K., C. K. Algar, A. E. Giblin, and J. J. Rich. 2015. Influence of organic carbon and nitrate loading on partitioning between dissimilatory nitrate reduction to ammonium (DNRA) and N2 production. Geochim. Cosmochim. Acta **164**: 146–160. doi:10.1016/j.gca.2015.04.049

Hellemann, D., P. Tallberg, I. Bartl, M. Voss, and S. Hietanen. 2017. Denitrification in an oligotrophic estuary: A delayed sink for riverine nitrate. Mar. Ecol. Prog. Ser. **583**: 63–80. doi:10.3354/meps12359

Hellemann, D., P. Tallberg, S. L. Aalto, M. Bartoli, and S. Hietanen. 2020. Seasonal cycle of benthic denitrification and DNRA in the aphotic coastal zone, northern Baltic Sea. Mar. Ecol. Prog. Ser. **637**: 15–28. doi:10.3354/meps13259

Hylén, A., S. J. van de Velde, M. Y. Kononets, M. Luo, E. Almroth-Rosell, and P. O. J. Hall. 2021. Deep-water inflow event increases sedimentary phosphorus release on a multi-year scale. Biogeosciences **18**: 2981–3004. doi:10.5194/bg-18-2981-2021

Jäntti, H., C. F. Stange, E. Leskinen, and S. Hietanen. 2011. Seasonal variation in nitrification and nitrate-reduction pathways in coastal sediments in the Gulf of Finland, Baltic Sea. Aquat. Microb. Ecol. **63**: 171–181. doi:10.3354/ame01492

Jäntti, H., and S. Hietanen. 2012. The effects of hypoxia on sediment nitrogen cycling in the Baltic Sea. Ambio **41**: 161–169. doi:10.1007/s13280-011-0233-6

Jensen, M. M., M. M. M. Kuypers, G. Lavik, and B. Thamdrup. 2008. Rates and regulation of anaerobic ammonium oxidation and denitrification in the Black Sea. Limnol. Oceanogr. **53**: 23–36. doi:10.4319/lo.2008.53.1.0023

Jickells, T. D., and others. 2017. A reevaluation of the magnitude and impacts of anthropogenic atmospheric nitrogen inputs on the ocean. Global Biogeochem. Cycl. **31**: 289–305. doi:10.1002/2016GB005586

Joye, S. B., and J. T. Hollibaugh. 1995. Influence of sulfide inhibition of nitrification on nitrogen regeneration in sediments. Science **270**: 623–625. doi:10.1126/science.270.5236.623

Kamp, A., S. Høgslund, N. Risgaard-Petersen, and P. Stief. 2015. Nitrate storage and dissimilatory nitrate reduction by eukaryotic microbes. Front. Microbiol. **6**: 1–15. doi:10.3389/fmicb.2015.01492

Kessler, A. J., K. L. Roberts, A. Bissett, and P. L. M. Cook. 2018. Biogeochemical controls on the relative importance of denitrification and dissimilatory nitrate reduction to ammonium in estuaries. Global Biogeochem. Cycl. **32**: 1–13. doi:10.1029/2018GB005908

Klawonn, I., S. Bonaglia, V. Brüchert, and H. Ploug. 2015. Aerobic and anaerobic nitrogen transformation processes in N2-fixing cyanobacterial aggregates. ISME J. **9**: 1456–1466. doi:10.1038/ismej.2014.232

Kononets, M. Y., and others. 2021. In situ incubations with Gothenburg benthic chamber landers: Applications and quality control. J. Mar. Syst. **214**: 1–20. doi:10.1016/j.jmarsys.2020.103475

Koreleff, F. 1983. Determination of nutrients, p. 125-187. In K. Grasshoff, M. Ehrhardt, and K. Kremling [eds.], Methods of seawater analysis. Verlag Chemie.

Kraft, B., H. E. Tegetmeyer, R. Sharma, M. G. Klotz, T. G. Ferdelman, R. L. Hettich, J. S. Geelhoed, and M. Strous. 2014. The environmental controls that govern the end product of bacterial nitrate respiration. Science **345**: 676–679. doi:10.1126/science.1254070

Kühl, M., C. Steuckart, G. Eickert, and P. Jeroschewski. 1998. A H2S microsensor for profiling biofilms and sediments: Application in an acidic lake sediment. Aquat. Microb. Ecol. **15**: 201–209.

Kuypers, M. M. M., H. K. Marchant, and B. Kartal. 2018. The microbial nitrogen-cycling network. Nat. Rev. Microbiol. **16**: 263–276. doi:10.1038/nrmicro.2018.9

Liblik, T., M. Naumann, P. Alenius, and others. 2018. Propagation of impact of the recent Major Baltic inflows from the Eastern Gotland Basin to the Gulf of Finland. Front. Mar. Sci. **5**: 1–23. doi:10.3389/fmars.2018.00222

Marzocchi, U., S. Bonaglia, S. J. van de Velde, P. O. J. Hall, A. Schramm, N. Risgaard-Petersen, and F. J. R. Meysman. 2018*a*. Transient bottom water oxygenation creates a niche for cable bacteria in long-term anoxic sediments of the Eastern Gotland Basin. Environ. Microbiol. **20**: 3031–3041. doi:10.1111/1462-2920.14349

Marzocchi, U., B. Thamdrup, P. Stief, and R. N. Glud. 2018*b*. Effect of settled diatom-aggregates on benthic nitrogen cycling. Limnol. Oceanogr. **63**: 431–444. doi:10.1002/lno.10641

Marzocchi, U., C. Thorup, A.-S. Dam, A. Schramm, and N. Risgaard-Petersen. 2021. Dissimilatory nitrate reduction by a freshwater cable bacterium. ISME J. **63**: 431–444. doi:10.1038/s41396-021-01048-z

McHatton, S. C., J. P. Barry, H. W. Jannasch, and D. C. Nelson. 1996. High nitrate concentrations in vacuolate, autotrophic marine *Beggiatoa* spp. Appl. Environ. Microbiol. **62**: 954–958.

Meier, H. E. M., G. Väli, M. Naumann, K. Eilola, and C. Frauen. 2018. Recently accelerated oxygen consumption rates amplify deoxygenation in the Baltic Sea. J. Geophys. Res. Ocean. **123**: 3227–3240. doi:10.1029/2017JC013686

Michiels, C. C., J. A. Huggins, K. E. Giesbrecht, J. S. Spence, R. L. Simister, D. E. Varela, S. J. Hallam, and S. A. Crowe. 2019. Rates and pathways of N2 production in a persistently anoxic fjord: Saanich inlet, British Columbia. Front. Mar. Sci. **6**: 1–23. doi:10.3389/fmars.2019.00027

Myllykangas, J.-P., T. Jilbert, G. Jakobs, G. Rehder, J. Werner, and S. Hietanen. 2017. Effects of the 2014 major Baltic inflow on methane and nitrous oxide dynamics in the water column of the Central Baltic Sea. Earth Syst. Dynam. **8**: 817–826. doi:10.5194/esd-8-817-2017

Nielsen, L. P. 1992. Denitrification in sediment determined from nitrogen isotope pairing. FEMS Microbiol. Ecol. **86**: 357–362.

Nilsson, M. M., and others. 2021. Particle shuttling and oxidation capacity of sedimentary organic carbon on the Baltic Sea system scale. Mar. Chem. **232**: 1–10. doi:10.1016/j.marchem.2021.103963

R Core Team 2020. R: A language and environment for statistical computing.

Revelle, W. 2020. psych: Procedures for psychological, psychometric, and personality research.

Revsbech, N. P. 1989. An oxygen microsensor with a guard cathode. Limnol. Oceanogr. **34**: 474–478. doi:10.4319/lo.1989.34.2.0474

Risgaard-Petersen, N., and S. Rysgaard. 1995. Nitrate reduction in sediments and waterlogged soil measured by 15N techniques, p. 287–295. *In* K. Alef and P. Nannipieri [eds.], Methods in applied soil microbiology and biochemistry. Academic Press.

Risgaard-Petersen, N., L. P. Nielsen, S. Rysgaard, T. Dalsgaard, and R. L. Meyer. 2003. Application of the isotope pairing technique in sediments where anammox and denitrification coexist. Limnol. Oceanogr. Methods **1**: 63–73. doi:10.4319/lom.2003.1.63

Robertson, E. K., K. L. Roberts, L. D. W. Burdorf, P. L. M. Cook, and B. Thamdrup. 2016. Dissimilatory nitrate reduction to ammonium coupled to Fe(II) oxidation in sediments of a periodically hypoxic estuary. Limnol. Oceanogr. **61**: 365–381. doi:10.1002/lno.10220

Robertson, E. K., and others. 2019. Application of the isotope pairing technique in sediments: Use, challenges and new directions. Limnol. Oceanogr. Methods. **17**: 112–136. doi:10.1002/lom3.10303

Rysgaard, S., N. Risgaard-Petersen, S. Niels Peter, J. Kim, and N. Lars Peter. 1994. Oxygen regulation of nitrification and denitrification in sediments. Limnol. Oceanogr. **39**: 1643–1652. doi:10.4319/lo.1994.39.7.1643

Sarmiento, J. L., and N. Gruber. 2006. Ocean biogeochemical dynamics. Princeton Univ. Press.

Schutte, C. A., A. Teske, B. J. MacGregor, V. Salman-Carvalho, G. Lavik, P. Hach, and D. de Beer. 2018. Filamentous giant Beggiatoaceae from the Guaymas Basin are capable of both denitrification and dissimilatory nitrate reduction to ammonium. Appl. Environ. Microbiol. **84**: 1–13. doi:10.1128/AEM.02860-17

Seitzinger, S. P., J. A. Harrison, J. K. Böhlke, A. F. Bouwman, R. Lowrance, C. Tobias, and G. van Drecht. 2006. Denitrification across landscapes and waterscapes: A synthesis. Ecol. Appl. **16**: 2064–2090.

Seitzinger, S. P., and others. 2010. Global river nutrient export: A scenario analysis of past and future trends. Global Biogeochem. Cycl. **24**: 1–16. doi:10.1029/2009GB003587

Senga, Y., K. Mochida, R. Fukumori, N. Okamoto, and Y. Seike. 2006. N_2O accumulation in estuarine and coastal sediments: The influence of H2S on dissimilatory nitrate reduction. Estuar. Coast. Shelf Sci. **67**: 231–238. doi:10.1016/j.ecss.2005.11.021

SMHI. 2021. SHARKweb. [accessed 2021 March 20]. Available from http://sharkweb.smhi.se.

Sommer, S., D. Clemens, M. Yücel, O. Pfannkuche, P. O. J. Hall, E. Almroth-Rosell, H. N. Schulz-Vogt, and A. W. Dale. 2017. Major bottom water ventilation events do not significantly reduce basin-wide benthic N and P release in the Eastern Gotland Basin (Baltic Sea). Front. Mar. Sci. **4**: 1–17. doi:10.3389/fmars.2017.00018

Song, G., S. Liu, J. Zhang, Z. Zhu, G. Zhang, H. K. Marchant, M. M. M. Kuypers, and G. Lavik. 2020. Response of benthic nitrogen cycling to estuarine hypoxia. Limnol. Oceanogr. **66**: 652–666. doi:10.1002/lno.11630

Sørensen, J., J. M. Tiedje, R. B. Firestone, J. Sorensen, J. M. Tiedje, and R. B. Firestone. 1980. Inhibition by sulfide of nitric and nitrous oxide reduction by denitrifying *Pseudomonas fluorescens*. Appl. Environ. Microbiol. **39**: 105–108.

Thamdrup, B., and T. Dalsgaard. 2002. Production of N2 through anaerobic ammonium oxidation coupled to nitrate reduction in marine sediments. Appl. Environ. Microbiol. **68**: 1312–1318. doi:10.1128/aem.68.3.1312-1318.2002

Thamdrup, B., and T. Dalsgaard. 2008. Nitrogen cycling in sediments, p. 527–568. *In* D. L. Kirchman [ed.]. Microbial ecology of the oceans.

Thornton, D. C. O. 2002. Diatom aggregation in the sea: Mechanisms and ecological implications. Eur. J. Phycol. **37**: 149–161. doi:10.1017/S0967026202003657

Tiedje, J. M., A. J. Sextone, and J. A. Robinson. 1983. Denitrification: Ecological niches, competition and survival. Antonie Van Leeuwenhoek **48**: 569–583. doi:10.1007/bf00399542

van de Velde, S. J., A. Hylén, U. Marzocchi, M. Leermakers, M. Y. Kononets, K. Choumiline, P. O. J. Hall, and F. J. R. Meysman. 2020. Elevated sedimentary removal of Fe, Mn and trace elements following a transient oxygenation event in the Eastern Gotland Basin, Central Baltic Sea. Geochim. Cosmochim. Acta **271**: 16–32. doi:10.1016/j.gca.2019.11.034

van den Berg, E. M., U. van Dongen, B. Abbas, and M. C. M. van Loosdrecht. 2015. Enrichment of DNRA bacteria in a continuous culture. ISME J. **9**: 2153–2161. doi:10.1038/ismej.2015.26

van Helmond, N. A. G. M., E. K. Robertson, D. J. Conley, M. Hermans, C. Humborg, W. K. Lenstra, and C. P. Slomp. 2020. Efficient removal of phosphorus and nitrogen in sediments of the eutrophic Stockholm Archipelago, Baltic Sea. Biogeosciences **17**: 2745–2766. doi:10.5194/bg-2019-376

Voss, M., H. W. Bange, J. W. Dippner, J. J. Middelburg, J. P. Montoya, and B. B. Ward. 2013. The marine nitrogen cycle: Recent discoveries, uncertainties and the potential relevance of climate change. Philos. Trans. R. Soc. B Biol. Sci. **368**: 1–11. doi:10.1098/rstb.2013.0121

Warembourg, F. R. 1993. Nitrogen fixation in soil and plant systems, p. 127–156. *In* R. Knowles and T. H. Blackburn [eds.]. Nitrogen isotope techniques.

Yücel, M., S. Sommer, A. W. Dale, and O. Pfannkuche. 2017. Microbial sulfide filter along a benthic redox gradient in the Eastern Gotland Basin, Baltic Sea. Front. Microbiol. **8**: 1–16. doi:10.3389/fmicb.2017.00169

Acknowledgments

We thank the crew of the University of Gothenburg's R/V *Skagerak* for support at sea and Bo Thamdrup for providing access to the GC–IRMS. Elin Almroth-Rosell, Lena Viktorsson, Madeleine Nilsson, Nils Ekeroth, Sebastiaan van de Velde, and Amanda Nylund kindly assisted during the fieldwork. This work was supported by the Swedish Research Council (VR grant 2015-03717 to POJH). UM was supported by the Grundfos Foundation.

Conflict of interest

None declared.

Submitted 07 April 2021
Revised 03 December 2021
Accepted 05 December 2021

Associate editor: Bradley D. Eyre